

Enabling Regional Explainability by Automatic and Model-agnostic Rule Extraction

Yu Chen^{1,2}, Tianyu Cui^{1,2}, Alexander Capstick^{1,2}, Nan Fletcher-Loyd^{1,2},
Payam Barnaghi^{1,2*}

¹Department of Brain Sciences, Imperial College London, London, United Kingdom.

²Care Research and Technology Centre, The UK Dementia Research Institute, London, United Kingdom.

*Corresponding author(s). E-mail(s): p.barnaghi@imperial.ac.uk;

Abstract

In Explainable AI, rule extraction translates model knowledge into logical rules, such as IF-THEN statements, crucial for understanding patterns learned by black-box models. This could significantly aid in fields like disease diagnosis, disease progression estimation, or drug discovery. However, such application domains often contain imbalanced data, with the class of interest underrepresented. Existing methods inevitably compromise the performance of rules for the minor class to maximise the overall performance. As the first attempt in this field, we propose a model-agnostic approach for extracting rules from specific subgroups of data, featuring automatic rule generation for numerical features. This method enhances the regional explainability of machine learning models and offers wider applicability compared to existing methods. We additionally introduce a new method for selecting features to compose rules, reducing computational costs in high-dimensional spaces. Experiments across various datasets and models demonstrate the effectiveness of our methods.

Keywords: Interpretability, Explainable Artificial Intelligence, Regional Rule Extraction, Decision-making

Explainable Artificial Intelligence (XAI) [1] has garnered increasing attention in recent years, driven by the widespread adoption of deep learning models. XAI generally aims to enable professionals to understand why a model has made a specific prediction (decision) and/or what a model has learned from the data. Rule extraction (also known as rule learning) [2, 3] is a field in XAI that translates a model's knowledge through a set of logical rules, such as IF-THEN statements, to obtain explainability of a model's reasoning. Such rule-based explanations can offer interpretations that mimic human experts' reasoning in solving knowledge-intensive problems [4]. This type of

interpretations are particularly desirable in applications with tabular data, such as drug discovery [5] and healthcare [6].

In practice, we often want to interpret a model's analysis over a specified subgroup of the data. For instance, interpreting the patterns captured by a model for diagnosing a specific disease is highly desirable in clinical applications (Figure 1(a)). Data samples labelled with the disease must share similar patterns that do not exist outside the specific subgroup. However, the subgroups of interest usually have sporadic occurrences in many real-world scenarios, including most applications that prefer rule explanations,

such as disease diagnosis, drug discovery, and financial fraud detection [7]. Existing methods in rule extraction focus on global explainability, often compromising regional explainability of minor subgroups of data to achieve better overall performance across the entire data distribution.

Regional rule extraction

To better interpret data patterns for a specified subgroup, we propose a novel method for regional rule extraction, which aims to extract optimal rules from a specified data region. Formally, the outcome of regional rule extraction from a model is in the form of IF-THEN statements: IF $x \in \mathbb{X}$, THEN $y \in \mathbb{Y}$, here \mathbb{X} denotes a subspace of a multivariate variable x confined by a set of rules, e.g. value ranges of several features. \mathbb{Y} denotes a subset of a target variable y . For instance, when extracting rules from a classifier, y often refers to the model's prediction and \mathbb{Y} denotes a class of interest (e.g. positive class in binary classification).

Compared to global rule extraction, regional rule extraction does NOT generate rules for the data region $y \notin \mathbb{Y}$. It is expected to gain two advantages through this reduction: i) obtaining more accurate and generalised rules for the specified data region $y \in \mathbb{Y}$, and ii) providing more precise control on key properties of the rules (e.g. number of rules, number of samples that satisfy these rules) for the specified data region.

A relevant topic in rule extraction is sequential covering, which iteratively learns a rule list for a data subgroup at each step to create a decision set that covers the entire dataset [9]. In sequential covering, the method applied to learn the rule list for a specified subgroup often involves a global rule extraction method, such as decision trees. The learned rules at each step then become the decision path to the purest node of the specified subgroup in a decision tree. To this end, regional rule extraction can be directly applied at each step of sequential covering to extract rules for specific data subgroups.

Implementation challenges

Conventional ways to extract rules for data subgroups or the entire dataset often utilise various search strategies, such as hill-climbing, beam

search, and exhaustive search [9], as the objective is to search the best subspace of features that significantly elevates the occurrence of data of interest. Due to the vastness of the search space, these strategies often require predefined discretisation for numerical features,

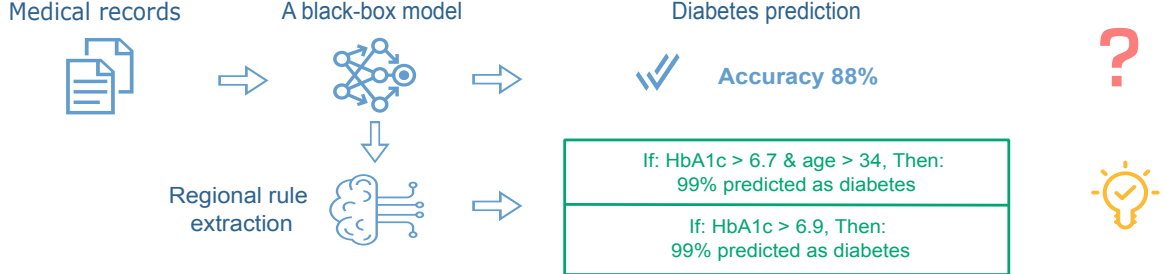
For instance, association rule classifiers [10, 11] use association rule mining [12, 13] to transform rule extraction into finding frequent item sets – groups of items that frequently appear together in training samples. Consequently, numerical features must be transformed to discretised items before this process. Similarly, KDRuleEx [14] was developed to extract decision tables using categorical features. Moreover, Falling rule list [15], Scalable Bayesian Rule Lists (SBRL) [16], and Bayesian Rule Sets (BRS) [17] are probabilistic rule extraction methods that use distributions of discrete variables for modelling rule generation.

However, predefined discretisation is often neither applicable nor desirable in real-world applications. Besides, when features are discretised individually, meaning the discretisation considers only the marginal distributions of features rather than their joint distributions, there is an implicit assumption that these features are independent – a condition not valid in many real-world scenarios. Moreover, the computational cost of automatic discretisation may increase exponentially when considering dependencies among a large number of features.

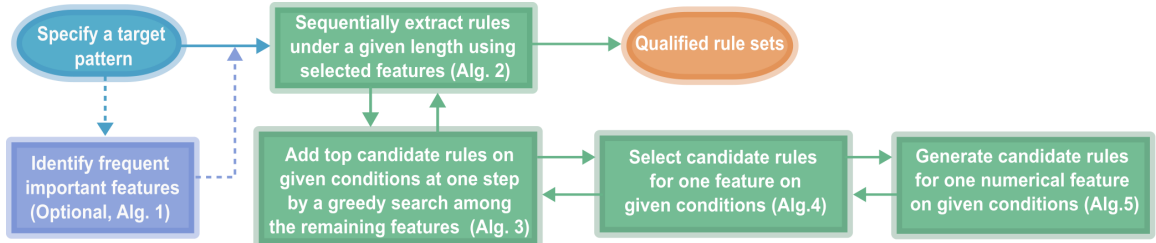
Decision Tree (DT) classifier [18, 19] is the most popular approach applied in rule extraction for neural networks due to its flexibility and accessibility [20–22]. The most attractive advantage of decision trees is their accessibility: they do not require predefined discretisation for numerical features. However, decision trees are not well-suited for regional rule extraction as: i) the selection of binary splits may still be affected by other data regions that are not of interest, especially in multi-mode scenarios; ii) the fact that they scan every observed value of a feature to find an optimal split, leading to a tendency to overfit the minimum support criterion on top features.

Automatic and Model-agnostic Regional Rule Extraction

In order to enable regional explainability with easy access, we propose *Automatic and Model-agnostic*



(a) An example scenario of applying regional rule extraction for diabetes prediction. The data region of interest is the region that contains samples predicted as positive diabetes cases by the model. The results are from our experiments on a diabetes prediction task [8]. In the extracted rules, Hemoglobin A1c (HbA1c) is a measure of a person’s average blood sugar level over the past 2-3 months.



(b) The workflow of our methods. Algorithm 1 is optional, depending on the dimensionality of the data.

Fig. 1: An overview of our method, illustrating the regional rule extraction and depicting the process pipeline.

Regional Rule Extraction (AMORE) – a novel approach that can automatically generate rules (e.g. key intervals of numerical features) through a model-agnostic algorithm. More specifically, our main contributions are three-fold:

- i) we enhance regional rule extraction for black-box machine learning models, offering more accurate and generalised rules for under-represented data regions than global rule extraction, and also allowing for local rule extraction for a given sample;
- ii) we enable automatic rule generation with numerical features, without requiring predefined discretisation or making any assumption about feature distributions;
- iii) we develop an efficient method for selecting features to compose rules, which is designed to seamlessly integrate with our rule generation method and reduce computational cost in high-dimensional feature spaces.

The workflow of our methods is illustrated in Figure 1(b). To the best of our knowledge, this is the first attempt to specifically address regional rule extraction with automated rule generation in the literature of XAI.

Results

We conducted experiments on several tasks with a set of publicly available datasets and various models to demonstrate the effectiveness of the proposed methods, including:

- i) diabetes prediction [8] using a *logistic regression model*;
- ii) sepsis prediction [23] using a *Neural Controlled Differential Equation (NCDE) model* [24];
- iii) molecular toxicity prediction [25] using a *Graph Neural Network (GNN)*;
- iv) handwriting digits (MNIST [26]) classification using a *Convolutional Neural Network (CNN)*;
- v) brain tumour MRI image classification [27] using an *EfficientNet* [28] pre-trained on ImageNet-1K dataset [29].

A summarised description of all tasks is provided in Table 1 in Supplementary material.

Most of these tasks are imbalanced binary classification, a common scenario in applications requiring rule explanation. As a result, we observe that models often exhibit significantly better

recall than precision even with techniques of up-weighting the minority class. In all these binary classification tasks, the positive class (i.e. $c = 1$) is designated as the class of interest. For obtaining a more balanced performance, we choose the prediction threshold y_{th} by maximising the difference between the True Positive Rate (TPR) and False Positive Rate (FPR) (i.e., TPR–FPR) using the ROC curve on the training set. Consequently, we consider the model predicting a positive sample when the model's output is greater than the threshold: $\hat{y}_p > y_{th}$, where \hat{y}_p represents the probability of a sample being from positive class given by the model. The MNIST and brain tumour MRI dataset are used to illustrate how our method can be applied to multi-classification tasks and how it can interpret image data through latent states. For both tasks, we select the class with the maximal \hat{y}_p as the predicted class. Although these experiments focus on classification tasks, the proposed method can be readily applied to regression tasks by transforming the target \mathbb{Y} from a discrete value to a value range of the target variable y .

Evaluation criteria

In the rest of this article, we denote the true label of a sample as y^* , the model's prediction as \hat{y} , the class of interest as the target class c , the sample index as n , the number of training samples as N , and the indicator function as $\mathbb{I}(\cdot)$. Since all the tasks are classification, we also refer to the specified data region of interest as the target region, denoted by $\hat{y} = c$.

We apply three criteria for evaluating the quality of an extracted rule set \mathbb{X} from a model:

1. *Support* – the number of training samples that satisfy the rule set. It is a metric for measuring the coverage of the rule set, acting a role like recall in classification evaluation. A larger support is not necessarily better as there is usually a trade-off between support and confidence.

$$\text{Support} = \sum_{n=1}^N \mathbb{I}(x^{(n)} \in \mathbb{X})$$

2. *Confidence* (also called rule accuracy) [11] – the proportion of samples that belong to the target region under the rule set. This metric quantifies the purity of the subspace defined

by the rule set. It can be computed as:

$$\text{Confidence} = \frac{\sum_{n=1}^N \mathbb{I}((\hat{y}^{(n)} = c) \& (x^{(n)} \in \mathbb{X}))}{\sum_{n=1}^N \mathbb{I}(x^{(n)} \in \mathbb{X})}$$

3. *Fitness* – a new metric we propose for regional rule extraction, being the ratio difference between samples that belong to the target region and those that do not, under the rule set, divided by the total number of samples in the target region. The higher the score, the better, and in the best case $\text{Fitness} = 1$:

$$\text{Fitness} = \frac{\sum_{n=1}^N \mathbb{I}((x^{(n)} \in \mathbb{X}) \& (\hat{y}^{(n)} = c))}{\sum_{n=1}^N \mathbb{I}(\hat{y}^{(n)} = c)} - \frac{\sum_{n=1}^N \mathbb{I}((x^{(n)} \in \mathbb{X}) \& (\hat{y}^{(n)} \neq c))}{\sum_{n=1}^N \mathbb{I}(\hat{y}^{(n)} = c)}$$

Support and confidence are widely applied in the literature of rule extraction. Typically, support and confidence are negatively correlated because including more samples likely introduces additional noise into the subspace. A better rule set should exhibit reduced correlation by increasing confidence while maintaining a similar support. We define *fitness* for evaluating regional rule sets, which takes into account the trade-off between support and confidence. This metric measures how well the subspace defined by a rule set fits into the target data region. A rule set with larger support and lower confidence, or one with smaller support and higher confidence, could both result in a lower fitness. Fitness can be negative when the subspace is mostly out of the target region.

Baseline method

In all of our experiments, we chose the Decision Tree (DT) classifier as the baseline method because, similar to our method, it does not require predefined discretisation for numerical features, and we were unable to find another method with this capability. Additionally, it allows us to verify the expected difference between the global and regional rule extraction.

The DT classifiers were trained to classify samples belonging to the target region as positive class and others as negative class. The rules from a DT classifier are formed by the decision path

Table 1: Rules extracted from different datasets and models by our method AMORE and Decision Tree (DT) classifier. In general, AMORE gives much higher confidence criteria than DT classifier while showing higher fitness even with less support than DT. The results suggest that our method gains a better trade-off between support and confidence for a regional explanation.

l_{max}	Rule properties	AMORE (Ours)	DT Classifier
Diabetes prediction			
1	Rules (\mathbb{X}) Target: $c = 1$	$\text{HbA1c_level} \geq 6.643$	$\text{HbA1c_level} > 6.349,$
	Support	2736	14501
	Confidence	0.993	0.515
	Fitness	0.202	0.033
Sepsis prediction			
2	Rules (\mathbb{X}) Target: $c = 1$	$\text{HR_ctime_t45} \geq 34,$ $\text{Temp_ctime_t38} \geq 34$	$\text{SBP_ctime_t22} > 9.5,$ $\text{Temp_ctime_t21} > 18.5$
	Support	2068	2000
	Confidence	0.860	0.846
	Fitness	0.205	0.19
Molecular toxicity prediction – AR			
2	Rules (\mathbb{X}) Target: $c = 1$	$1.149 \leq \text{NumAliphaticRings} \leq 10.405,$ $\text{SMR_VSA5} \geq 0.167$	$\text{NumAliphaticRings} > 1.414,$ $\text{SMR_VSA5} > 0.836$
	Support	326	253
	Confidence	0.801	0.874
	Fitness	0.235	0.227
Molecular toxicity prediction – AhR			
2	Rules (\mathbb{X}) Target: $c = 1$	$1.631 \leq \text{NumAliphaticCarbocycles} \leq 4.679,$ $1.341 \leq \text{fr_bicyclic} \leq 5.643$	$\text{NumAliphaticRings} > 1.414,$ $\text{SlogP_VSA4} > 2.059$
	Support	158	184
	Confidence	0.898	0.81
	Fitness	0.247	0.223
MNIST digit classification			
2	Rules (\mathbb{X}) Target: $c = 7$	$z_{44} \geq 6.223,$ $0 \leq z_{114} \leq 3.105$	$z_{44} \geq 6.429,$ $z_{114} \leq 3.463$
	Support	5340	5518
	Confidence	0.900	0.891
	Fitness	0.682	0.687
Brain tumour MRI classification			
2	Rules (\mathbb{X}) Target: $c = 2$	$z_{1200} \geq 0.653,$ $-0.208 \leq z_{1110} \leq -0.007$	$z_{115} > 0.781$
	Support	301	274
	Confidence	0.934	0.934
	Fitness	0.853	0.778

to the node with the highest fitness. The rules from AMORE are the rule set with the highest fitness among all candidate rule sets. All results are provided in Table 1.

Results from AMORE are deterministic when both the model and training set remain unchanged. Similarly, the DT classifier yields consistent results upon varying the random seeds, as all features are involved in split selection in decision trees. Therefore, there is no variance reported in Table 1.

Hyperparameters

In general, there are two hyperparameters required to constrain the extracted rules: i) the maximum number of features included in a rule set is limited by l_{max} , constraining the complexity of extracted rules to not be too large; ii) the minimum number of training samples that satisfy the extracted rules is limited by s_{min} , constraining the support of the rules to not be too small. We configure the same l_{max} for both methods in each task for consistency. However, the hyperparameter s_{min} is highly correlated to the optimal fitness that a rule set can achieve. Therefore, we conducted a grid search for s_{min} , alongside

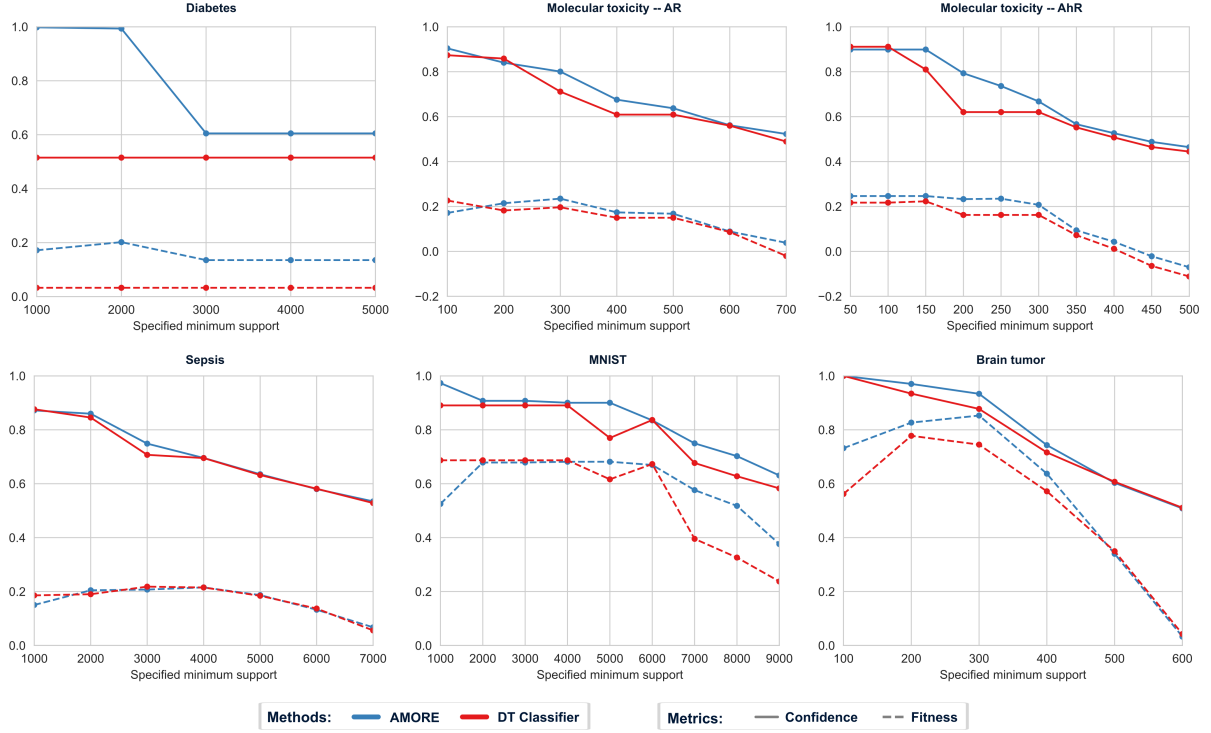


Fig. 2: Comparing AMORE and DT classifiers while specifying the same minimum support, s_{min} , on the x axis and fixing the l_{max} as in Table 1 for each task. We choose the range of s_{min} according to the size of target region for each task. We perform a grid search for other hyperparameters for both methods in all cases and compare the confidence and fitness of their best rule sets. We observe that AMORE generally yields better or equivalent results compared to the DT classifier.

other method-specific hyperparameters, for both methods in each task. We provide the selected hyperparameters for both methods in Table 2 in Supplementary Material. Figure 2 visualises the comparison between the two methods while specifying different values of s_{min} .

To avoid selecting rules that have slightly higher fitness but significantly lower confidence, we specify a *confidence lower bound* ι for choosing the best rule set across all experiments. This lower bound filters out any rule sets with confidence levels below it when selecting the best rule set based on fitness. However, if no rule set with a confidence above this lower bound is obtained, we simply select the one with the highest fitness. To verify the robustness of AMORE with respect to ι , we conducted a sensitivity analysis by varying ι from 0.7 to 0.9 (Figure 1 in Supplementary Material). AMORE maintained better or equivalent performance compared to DT classifiers. We chose

$\iota = 0.8$ as it is considered reasonably good for rule confidence while allowing a higher support.

Task 1 – Diabetes prediction

The Diabetes prediction dataset is a public dataset [8] that contains medical and demographic information of 100,000 patients along with their diabetes status. It consists of eight raw features including two binary features (`hypertension`, `heart disease`), two categorical features (`gender`, `smoking history`), and four numerical features (`age`, `BMI`, `HbA1c_level`, and `blood glucose level`).

We trained a logistic regression model to classify whether a patient has diabetes or not, and then applied our methods to extract rules that interpret the key knowledge acquired by the model in recognising diabetes patients. We first identify highly influential features using our feature selection method (Algorithm 1) and then extract

Table 2: Rules extracted by AMORE for interpreting predictions of individual test samples in the diabetes dataset. We set $s_{min} = 1000$, $l_{max} = 3$ for all test samples. The prediction threshold y_{th} is 0.457. The rules exhibit lower confidence and fitness when \hat{y}_p is lower, indicating that the purity of a local subspace correlates with the model’s uncertainty.

	Test sample 1	Test sample 2	Test sample 3
Predicted probability	$\hat{y}_p = 0.908$	$\hat{y}_p = 0.591$	$\hat{y}_p = 0.424$
Rules (X) Target: $\hat{y} = c$	<code>HbA1c_level</code> ≥ 6.25 , <code>blood_glucose_level</code> ≥ 190 , <code>age</code> > 40	<code>HbA1c_level</code> ≥ 5.071 , <code>blood_glucose_level</code> ≥ 174.286 , $33.384 \leq \text{BMI} \leq 45.071$	<code>HbA1c_level</code> ≥ 5.253 , <code>age</code> > 54 , <code>BMI</code> ≥ 37.48
Support	1967	1128	1340
Confidence	1.	0.974	0.893
Fitness	0.147	0.08	0.079

rules for the target region using those features. The most informative feature identified by both methods is HbA1c level (`HbA1c_level`). As a measure of a person’s average blood sugar level over the past 2-3 months, it reasonably emerges as a key factor in predicting diabetes, demonstrating the effectiveness of our feature selection method. As only one rule is allowed in this task, AMORE achieved much better performance than the decision tree classifier (Table 1) due to the trade-off issue in global rule extraction is magnified in such scenarios.

Furthermore, we demonstrate obtaining local rules for three test samples by our method, as shown in Table 2: one with a very high predicted probability, another close to the decision threshold, and a third below the threshold. The obtained local rules exhibit lower confidence and fitness when the predicted probability is lower, indicating that the quality of local rules correlates with the model’s uncertainty on the given sample. For samples that are distant from the target region (e.g. $\hat{y}_p \approx 0$), our approach may not return valid local rules (rules that give a higher confidence than without them).

Task 2 – Sepsis prediction

The Sepsis dataset [23] is a public dataset consisting of hourly vital signs and lab data, along with demographic data, for 40,336 patients obtained from two distinct U.S. hospital systems. The objective is to predict the onset of sepsis within 72 hours from the time a patient has been admitted to the ICU. We treat the data as time series, with each data sample comprising 72 time steps (hours), and each time step including 34 features representing vital signs and laboratory data. For

patients who do not have records for the full 72 hours, we treated features of missing hours as missing values filled by NaN before feature augmentation.

We conducted feature augmentation by three cumulative operations on the 34 original features: i). `feature_ct` denotes the cumulative number of time steps that a raw feature has non-missing values; ii). `feature_cmax` denotes the maximum value of a specific feature among all passed time steps; iii). `feature_csum` denotes the value sum of a specific feature over passed time steps. We added the time index as a suffix to the augmented feature. For example, `HR_ct_t45` denotes the cumulative number of time steps that have recorded `Heart Rate` (beats per minute) at the 45-th time step. After augmentation, each time step has 136 features, resulting in a total of 9,792 features for each sample.

We trained a Neural Controlled Differential Equation (NCDE) model [24] on this dataset to predict the onset of sepsis. NCDE is able to deal with irregular sampled time series using controlled differential equations. Ordinary Differential Equation (ODE) solvers are involved in the approximation of the gradients of the model parameters. This way, we demonstrate that our approach can also be applied to this type of models. More information about NCDE can be found in Supplementary Materials.

The extracted rules can be found in Table 1. The feature `Temp` indicates temperature ($^{\circ}\text{C}$) and `SPB` is Systolic BP (mm Hg). As this task has a high dimensional feature space, our method selected different features with decision trees. We also observe that the top rules of both methods are from features augmented by cumulative time steps. This suggests that the model considers the

frequency of taking those vital signs and lab tests as key information for predicting sepsis.

Task 3 – Molecular toxicity prediction

Predicting the toxicity of new medicines using molecular structure is crucial in drug discovery, given that over 30% of promising pharmaceuticals fail in human clinical trials due to toxicity discovered in animal models [30]. The Tox21 (The Toxicology in the 21st Century) challenge contained in the MoleculeNet [25] is a public dataset that assesses the toxicity of 8,014 compounds across 12 different categories. These categories include 7 nuclear receptors and 5 stress response pathways.

We trained a graph attention network [31] to predict the categories of compounds using their chemical structures as input. This is a multi-label classification task, and we chose the first two categories for rule extraction as demonstration: the androgen receptor (AR) and aryl hydrocarbon receptor (AhR). We utilise RDKit descriptors [32] to map molecule structures to interpretable features, providing a consistent set of features that describe essential molecule properties. As the results presented in Table 1, AMORE obtained higher fitness than DT classifiers in both cases.

Task 4 –MNIST digits classification

In addition to tabular data, we showcase the capability of our method to interpret models for image data by using MNIST dataset [26]. We trained a neural network with a convolutional layer and two fully connected layers for this task. The target region is set to $\hat{y} = 7$, which identifies the model’s key knowledge for classifying the digit 7. We used the model’s latent representations (input to the final linear layer) as features to generate rules, which dimension is 128. The performance of extracted rules can be found in Table 1 as well. For a visual demonstration, we illustrate the extracted rules by samples that satisfy each rule in Figure 3(a). It is clear to see that the first rule emphasises the upper half of digit 7, while the second rule focuses on the lower half.

Task 5 – Brain tumour MRI classification

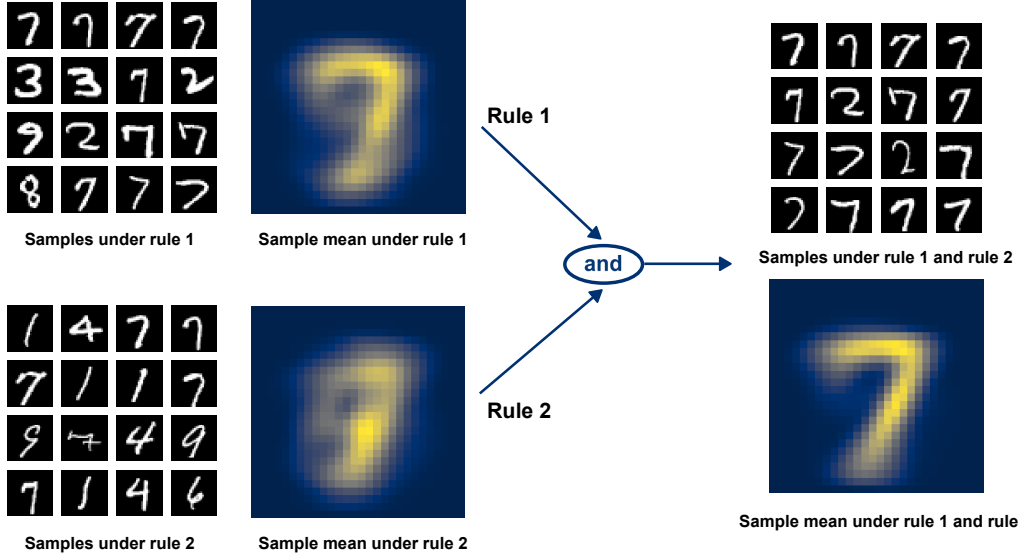
The brain tumour MRI dataset [27] is a public dataset that includes brain MRI images with four classes: *glioma tumour*, *meningioma tumour*, *pituitary tumour*, and *normal*. We used an EfficientNet [28] architecture for this classification task which is pre-trained on ImageNet-1K dataset [29].

Like the MNIST task, we also use the latent representations from the model as features to generate rules for a target region in this experiment, which dimension is 1280. We extracted rules for identifying “normal” brain MRI images where the class “normal” is the minority class in this dataset. The sample means of the MRI images are not visually interpretable. Therefore, we showcase two samples that satisfy rules extracted by AMORE in Figure 3(b): one is from class “normal” and the other is malignant. We visualise each rule by colouring pixels according to each pixel’s impact on the latent feature that defines the rule, thereby highlighting the most impactful areas for each rule in an MRI image.

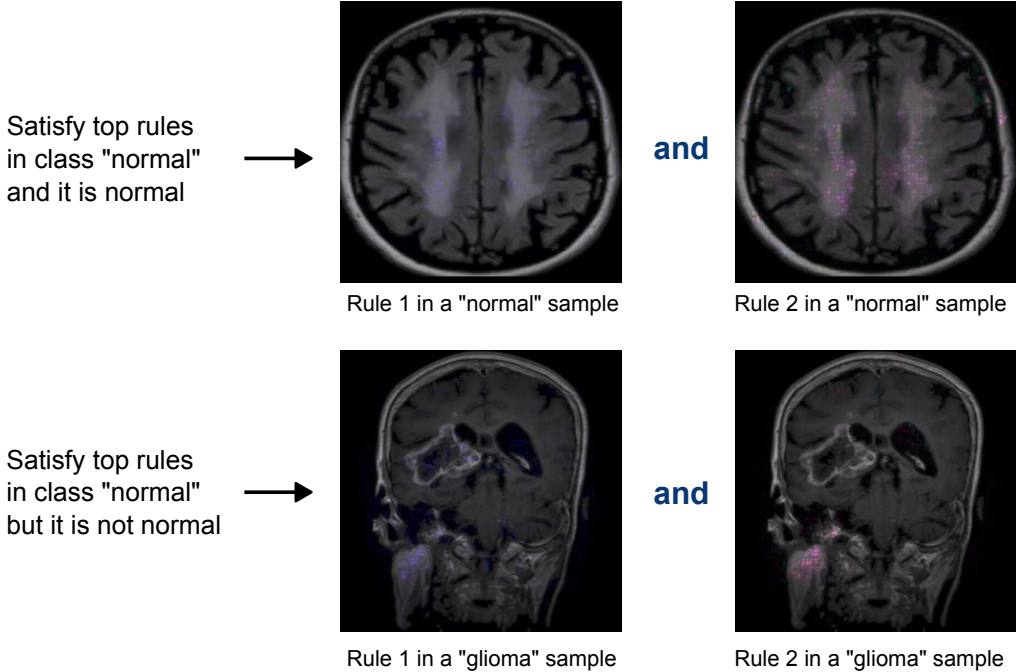
Discussion

In the presented experiments, we illustrate that AMORE can extract representative rules with large support and high confidence for specific target regions, achieving better or equivalent performance compared to DT based explanation. Our proposed approach is also applicable to a broad range of machine learning models without requiring predefined discretisation for numerical features. We compare the best rule sets with only “AND” operations here, however, a more comprehensive view could be constructed by post-processing that merges candidate rule sets using “OR” operations according to customised requirements. We consider this as future work.

While two hyperparameters are configured to limit the minimum support (s_{min}) and the maximum length (l_{max}) of extracted rules for both methods, we observe that the rules extracted by AMORE often have actual support and length that are closer to these configurations. This aligns with our expectations to have more precise control over regional rule extraction.



(a) Visualisation of extracted rules from the MNIST dataset. Here, rule 1 is $z_{44} \geq 6.223$ and rule 2 is $0 \leq z_{114} \leq 3.105$ as in Table 1.



(b) Visualisation of extracted rules from brain tumour MRI dataset by two samples that satisfy the extracted rules of class "normal". The above row is a sample truly "normal" and the below row is a sample not labelled as "normal". The first column highlights pixels that have higher contributions to the latent state (z_{1200}) in rule 1 ($z_{1200} \geq 0.653$) and the second row is for the latent state (z_{1110}) in rule 2 ($-0.208 \leq z_{1110} \leq -0.007$). We visualise the latent state of each rule by colouring pixels according to their impact scores for the latent state, highlighting highly impactful regions of each rule in the figures.

Fig. 3: Visualisation of extracted rules for both image datasets.

We demonstrated how to apply AMORE with data types other than tabular data in several

experiments. For instance, in the molecular toxicity prediction task, we map the molecular

structures to RDKit descriptors, providing interpretable rules by the descriptors. Likewise, in the MNIST and Brain tumour experiments, we extract rules from the latent space of models and then interpret them through visualisation in the raw pixel space. In general, for data with features that are not directly comprehensible in the form of rules, one can map the raw features to an interpretable feature space so that AMORE can be applicable. For instance, the speech and text data can be interpreted by mapping raw features to semantic concepts, taking into account specific requirements of domain knowledge for an application.

Regarding regression and unsupervised tasks with continuous target variables, AMORE can be applied to extract rules by defining a value range of the target variable as the target region. However, AMORE is not intended to reveal the dynamic patterns of continuous variables in regression tasks, such as patterns indicating an increase or decrease in the variable. Future work may focus on the use of the dynamics (e.g., the first or second-order derivatives) of the target variable instead to enable extracting rules for dynamic patterns.

Methods

The objective of regional rule extraction is to find a subspace of data that maximises the purity of a specified subgroup within it. The subspace is defined by a rule set that must satisfy two constraints: the maximum length l_{max} and the minimum support s_{min} . We quantify the purity of a specified subgroup as its conditional probability within that subspace, which can be formulated as below:

$$\begin{aligned} & \arg \max_{\mathbb{X}} \Pr(y \in \mathbb{Y} | x \in \mathbb{X}) \\ \text{s.t. } & |\mathbb{X}| \leq l_{max}, \quad \sum_{n=1}^N \mathbb{I}(x^{(n)} \in \mathbb{X}) \geq s_{min} \end{aligned} \quad (1)$$

Where $|\mathbb{X}|$ denotes the length of the rule set. We define one rule by one feature, i.e. one value of a categorical feature or one value interval of a numerical feature. The length of the rule set is the number of features included in the rule set.

It is computationally prohibitive to solve such an optimisation problem exactly, especially for

numerical features in high-dimensional space. The challenges are mainly due to: i) large search space for selecting feature combinations to compose rules; ii) large search space for selecting value intervals of numerical features. We tackle these challenges heuristically through two procedures: i) a feature selection procedure, and ii) a rule extraction procedure.

Feature selection for rule extraction

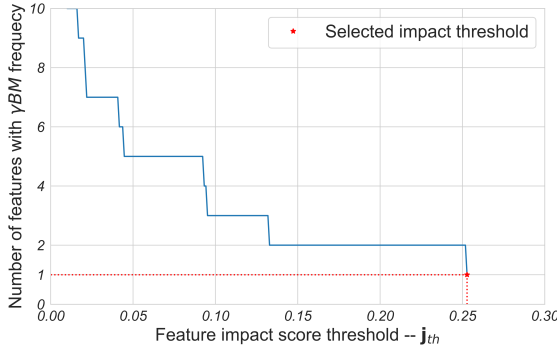
Although the feature selection procedure is optional, we recommend conducting it before rule extraction for high-dimensional data. To align with the purpose of rule extraction, we focus on selecting features that frequently appear in a decision path, aligning with the principles of decision-making. This can be achieved by using feature importance measures to identify the most influential features for given samples and then mining frequent, highly important feature sets across those samples.

We propose a new method (Algorithm 1) for effectively selecting features of rules. It can be performed using any feature importance measures. Nonetheless, we have also designed a new measurement (Equation (3)) for differentiable models, leveraging integrated gradients [33] to quantify feature importance as it can better align with the principle of decision rules. For non-differentiable models, such as tree models or ensemble models, one can use SHAP [34] or LIME [35] to measure feature importance.

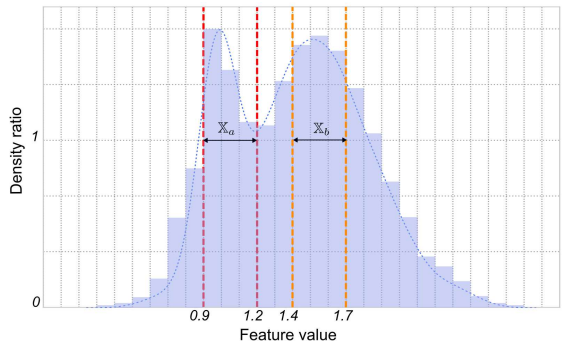
Preliminary: integrated gradients

The integrated gradients (also known as integrated Jacobian) [33, 36] is a pairwise measure that can quantify the contribution of changing an input feature on the shift of a target variable given by a trained differentiable model. This measure can be applied to identify feature sets that most frequently have a joint high impact on shifting a target variable, which is crucial for determining the target variable's value.

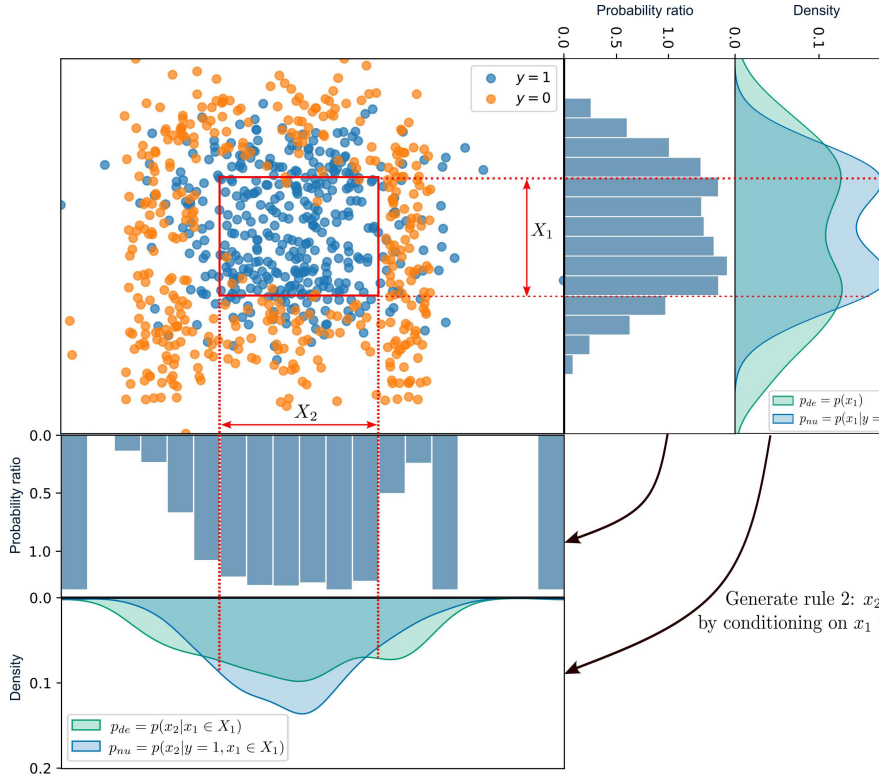
Assume we have a model $\mathcal{G} : \mathbb{R}^D \rightarrow \mathbb{R}$ to infer a variable $y \in \mathbb{R}$ by an observation $x \in \mathbb{R}^D$, i.e. $y = \mathcal{G}(x)$. Here D is the number of features. Let x_i denote the i -th feature of a baseline sample x , \tilde{x}_i denote the i -th feature of a test sample \tilde{x} . We can compute the integrated gradient of the i -th feature with respect to the shift of y between the



(a) Demonstration of selecting feature contribution threshold j_{th} that satisfy Equation (4) by stepwise scanning.



(b) Illustration of generating feature intervals in a multi-mode scenario. We can capture both modes by initialising two intervals with the two peak grids.



(c) Demonstration of the automatic rule generation with numerical features. This figure was plotted with synthetic data of two classes in a 2-dimensional feature space. The target region is set as $y = 1$. We generate the first rule by identifying the mode interval of the probability ratio on the feature represented by the vertical axis. The second rule for the feature on the horizontal axis is generated by conditioning on the first rule. We applied KDE for plotting density curves, the histograms of probability ratios and the subspace in the red rectangle were obtained through our method. More details can be found in Algorithms 4 and 5.

Fig. 4: Visualisation of the threshold selection and feature interval searching.

two samples as below [33, 36]:

$$\mathbf{j}_i = (x_i - \tilde{x}_i) \int_0^1 \frac{\partial \mathcal{G}(x)}{\partial x_i} \Big|_{x=\gamma_i(\lambda)} d\lambda, \quad (2)$$

$$\gamma_i(\lambda) = \tilde{x}_i + \lambda(x_i - \tilde{x}_i), \quad \forall \lambda \in [0, 1]$$

Here $\gamma_i(\lambda)$ represents a point between x_i and \tilde{x}_i .

Feature importance measured by integrated gradients

Based on Equation (2), we then estimate the importance of the i -th input feature on the shift of y as the following equation:

$$\tilde{\mathbf{j}}_i = \left| \frac{\mathbf{j}_i}{y - \tilde{y}} \right|, \quad \text{where } y = \mathcal{G}(x), \quad \tilde{y} = \mathcal{G}(\tilde{x}) \quad (3)$$

In brief, $\tilde{\mathbf{j}}_i$ represents the ratio of the shift attributed to the i -th feature out of the total shift caused by all features.

As the original integrated gradients are sensitive to the scale of the target variable, we normalise the integrated gradients by the absolute value of the shift of the target variable. This normalisation ensures that the importance of each feature is comparable across different sample pairs, which is crucial for identifying frequently important feature sets.

Since this feature importance is measured using the shift between a baseline sample and a test sample, we suggest choosing class centres as baseline samples in classification tasks. Test samples should be a randomly selected subset from the training set to simulate decisions about the class origin of a random sample. We ensure the test samples are balanced across all classes, preventing the oversight of important features for minor subgroups of data. For regression or unsupervised tasks, the selection of baseline samples could depend on the specific application. A few general options are the mean, median, or mode of the training samples clustered by target regions.

Frequently important feature sets

The proposed feature importance (Equation (3)) is measured by a pair of samples: a baseline sample and a test sample. When given B baseline samples, M test samples, and D features for each sample, one can produce an importance matrix $\mathbf{J} \in \mathbb{R}^{B \times M \times D}$. For instance, $\mathbf{J}_{b,m,i}$ is the importance of the i -th feature on the shift of the target variable from the b -th baseline sample to the m -th test sample. This importance matrix \mathbf{J} can be readily transformed to a size of $BM \times D$. For feature importance determined by other measures, one may directly construct the importance matrix of size $N \times D$, where N is the number of samples.

Then each row of the importance matrix \mathbf{J} can then be transformed into a sequence of feature indices, containing indices of features with an importance score greater than a threshold \mathbf{j}_{th} . Through this transformation, we are able to apply the FP-Growth algorithm [37] to discover subsets of features that frequently have a high impact together. FP-Growth is an efficient algorithm for mining frequent item sets (i.e. items frequently appear in the same records). Here we treat a feature index as an item and one sequence as one record.

The impact threshold \mathbf{j}_{th} is a key parameter for filtering less important features. If it is too small, too many less important features may be included. If it is too large, there may be not enough features that satisfy the minimum frequency requirement. In principle, we prefer a threshold that can provide enough features and be as high as possible. To determine the threshold automatically, we suggest selecting it by the following equation:

$$\sum_{i=1}^D \mathbb{I} \left(\left(\sum_{b=1}^B \sum_{m=1}^M \mathbb{I}((\mathbf{J}_{b,m,i} \geq \mathbf{j}_{th})) \right) \geq \gamma BM \right) = 1, \quad (4)$$

This equation requires the threshold \mathbf{j}_{th} to be sufficiently large so that only one feature can have an impact score larger than \mathbf{j}_{th} in at least γBM rows of the importance matrix \mathbf{J} , where $\gamma \in (c_{min}/BM, 1]$, and c_{min} is the minimum occurrence of a frequent set. For instance, when $\gamma = 1$, it requires that the most frequent feature has impact scores larger than \mathbf{j}_{th} for all samples, similar to the root node of a decision tree. We set $\gamma = 0.99$ in all of our experiments. When γ is smaller, \mathbf{j}_{th} will be higher, and more features will be filtered out. Our implementation uses a stepwise scanning process to find the threshold. As illustrated in Figure 4(a), we initialise the threshold with a small value and increase it stepwise until only one feature has a frequency no less than γBM (Equation (4)). It is clear to see that the number of features that satisfy the γBM frequency requirement decreases as the threshold increases. In this way, we ensure that the threshold is appropriate to include sufficiently representative features for rule extraction. The pseudo-code of feature selection is described in Algorithm 1.

In FP-Growth algorithm, a frequent item set should have appeared at least c_{min} times among

all records. Additionally, it is often required to include fewer than k_{max} items. This requires c_{min} and k_{max} as two hyperparameters for the FP-Growth algorithm. c_{min} is determined by the least frequent item in a frequent item set, so we suggest a relatively small value for it, such as 10% of the training size. The use of threshold j_{th} automatically limits the number of items in a frequent item set, so we just set k_{max} to be large enough to encompass the longest item set. When there are multiple frequent item sets discovered, we choose the longest one, and if there are ties, we choose the most frequent one as the candidate feature set for rule extraction.

Algorithm 1 FrequentFeaturesSelection

Input: X_b – baseline samples, X_t – test samples, \mathcal{G} – a model producing the target variable y , c_{min} – minimum frequency of a frequently important feature set, k_{max} – maximum length of a frequently important feature set.

$\mathbf{J} \leftarrow$ generate the importance matrix by X_b , X_t , \mathcal{G} (Equations (2) and (3)),
 $j_{th} \leftarrow$ decide the threshold of impact score (Equation (4)),
 $\mathbf{F} \leftarrow$ transform \mathbf{J} to a set of feature sequences, each sequence contains the indices of features having an impact score larger than j_{th} ;
 $F_{fq} \leftarrow$ obtain frequently important feature sets by FP-Growth(\mathbf{F} , c_{min} , k_{max}) [37]
 $F_{fq}^* \leftarrow$ the longest feature set in F_{fq} , if there are ties, choose the most frequent one;
Return: F_{fq}^*

Automatic and Model-agnostic Regional Rule Extraction (AMORE)

After obtaining the frequently important feature set by using Algorithm 1, the next step is to identify a subset of these features, with a length $\leq l_{max}$, and determine the value ranges of those features that can maximise the conditional probability in Equation (1). We can explicitly decompose the overall condition to each selected feature, i.e. $\{x \in \mathbb{X}\} \triangleq \{x_{f_1} \in \mathbb{X}_{f_1}, \dots, x_{f_l} \in \mathbb{X}_{f_l}\}$, where $\{f_1, \dots, f_l\}$ are the indices of selected features, \mathbb{X}_{f_i} ($\forall 1 \leq i \leq l$) denotes a value range of f_i -th feature. According to the chain rule of conditional probability, we can then approximate the conditional

Algorithm 2 ExtractRuleSets

Input: X – features of training samples; Y – indicator of the target region $y \in \mathbb{Y}$, which is a binary vector; F_{fq}^* – the selected feature set; s_{min} – minimum support of a rule set; l_{max} – maximum length of a rule set; n_g – number of value grids for numerical features; K – maximum number of candidate rules added at each step.

$\mathcal{R}_{tree} \leftarrow$ Initialise a tree structure for storing candidate rule sets,

$\mathcal{X}_{l_{max}}^0 \leftarrow$ Initialise previous rules by domain of x ,
Start adding rules from the root node, see Algorithm 3.

$\text{AddRules}(\mathcal{R}_{tree.root}, F_{fq}^*, X, \mathbb{Y}, \mathcal{X}_{l_{max}}^0, s_{min}, n_g, l_{max}, K)$,

$\mathbb{R}_{sets} \leftarrow$ Obtain all candidate rule sets in \mathcal{R}_{tree}

Return: \mathbb{R}_{sets}

probability of regional rule extraction as below:

$$\begin{aligned} & \Pr(y \in \mathbb{Y} | x_{f_1} \in \mathbb{X}_{f_1}, \dots, x_{f_l} \in \mathbb{X}_{f_l}) \\ & \propto \prod_{i=1}^l \frac{\Pr(x_{f_i} \in \mathbb{X}_{f_i} | y \in \mathbb{Y}, x \in \mathcal{X}_l^{i-1})}{\Pr(x_{f_i} \in \mathbb{X}_{f_i} | x \in \mathcal{X}_l^{i-1})} \\ & \{x \in \mathcal{X}_l^{i-1}\} \triangleq \{x_{f_1} \in \mathbb{X}_{f_1}, \dots, x_{f_{i-1}} \in \mathbb{X}_{f_{i-1}}\}, \\ & \forall 1 < i \leq l, \quad \mathcal{X}_l^0 \triangleq \text{dom}(x) \end{aligned} \quad (5)$$

\mathcal{X}_l^{i-1} denotes conditions composed by previous $i-1$ features. We treat this decomposition as a sequence of operations. In the i -th operation, we select the value range of f_i -th feature that maximises a probability ratio \mathbf{r}_{f_i} , where \mathbf{r}_{f_i} is defined as the following:

$$\mathbf{r}_{f_i} \triangleq \frac{\Pr(x_{f_i} \in \mathbb{X}_{f_i} | y \in \mathbb{Y}, x \in \mathcal{X}_l^{i-1})}{\Pr(x_{f_i} \in \mathbb{X}_{f_i} | x \in \mathcal{X}_l^{i-1})} \quad (6)$$

Through this decomposed objective for each feature, we can obtain candidate rules one by one for a given order of features. However, the result is not guaranteed to be globally optimal if we do not search all possible orders and value ranges of features. As it is usually computationally prohibitive to find the exact global optimal solution, a feasible way is to select the feature f_i that has the maximum \mathbf{r}_{f_i} among all remaining features in the frequently important feature set at the i -th step, which is analogous to adding branches in decision

Algorithm 3 AddRules

Input: ν_{par} – parent rule node; $F_{f_q}^*$ – the selected feature set; X – features of training samples; Y – indicator of the target region $y \in \mathbb{Y}$, which is a binary vector; \mathcal{X}_{pre} – previous rules; s_{min} – minimum support of a rule set; l_{max} – maximum length of a rule set; n_g – number of value grids for numerical features; K – maximum number of candidate rules added at each step.

```

 $\tilde{F}_{f_q}^* \leftarrow$  Remove the feature of the parent rule node
 $\nu_{par}$  in  $F_{f_q}^*$ ,
if  $\tilde{F}_{f_q}^*$  is not empty then
     $\mathbb{X}_K^* \leftarrow$  obtain candidate rules for each feature in
     $\tilde{F}_{f_q}^*$ , and select the top  $K$  rules with highest ratios,
    see Algorithm 4 for getting candidate rules for one
    numerical feature.
    for  $\mathbb{X}_{f_i}^* \in \mathbb{X}_K^*$  do
         $\nu_{new} \leftarrow$  Create a new rule node by  $\mathbb{X}_{f_i}^*$ ,
         $\tilde{\mathcal{X}}_{pre} \leftarrow$  Update  $\mathcal{X}_{pre}$  by adding  $\mathbb{X}_{f_i}^*$ .
        if  $len(\tilde{\mathcal{X}}_{pre}) < l_{max}$  then
            AddRules( $\nu_{new}$ ,  $\tilde{F}_{f_q}^*$ ,  $X$ ,  $\mathbb{Y}$ ,  $\tilde{\mathcal{X}}_{pre}$ ,  $s_{min}$ ,
             $n_g$ ,  $l_{max}$ ,  $K$ )
        end if
    end for
end if

```

trees. This approach can achieve a global optimal solution when the features are independent of each other, as the order of features does not matter in such cases.

Without any assumptions about the conditional distributions, we estimate the ratio \mathbf{r}_{f_i} using training samples as below:

$$\mathbf{r}_{f_i} \approx \frac{\sum_{n=1}^N \mathbb{I}(x^{(n)} \in \mathcal{X}_l^{i-1})}{\sum_{n=1}^N \mathbb{I}(x_{f_i}^{(n)} \in \mathbb{X}_{f_i} \text{ & } x^{(n)} \in \mathcal{X}_l^{i-1})} \times \frac{\sum_{n=1}^N \mathbb{I}(x_{f_i}^{(n)} \in \mathbb{X}_{f_i} \text{ & } (x^{(n)}, y^{(n)}) \in (\mathcal{X}_l^{i-1}, \mathbb{Y}))}{\sum_{n=1}^N \mathbb{I}((x^{(n)}, y^{(n)}) \in (\mathcal{X}_l^{i-1}, \mathbb{Y}))} \quad (7)$$

One advantage of using this probability ratio as our stepwise objective is that we can directly discard candidate rules with a ratio not larger than 1 because it does not increase the overall conditional probability in Equation (5).

We provide detailed pseudo code of this process in Algorithms 2 and 3. The input argument n_g

is the number of grids for initialising value intervals of numerical features, which will be explained in Algorithm 4. K is the maximum number of candidate rules that can be added at each step. We may obtain multiple rule sets when $K > 1$ to cope with multi-mode scenarios in data distributions. Note that there may be fewer than K rules added at each step as we discard rules with a ratio not larger than 1. We set $K = 3$ in all of our experiments.

Generating rules for numerical features

To generate candidate rules for categorical features, each category can be considered as a candidate for the designated rule. However, it is not trivial to generate candidate rules for numerical features. The question here is how to automatically identify intervals of numerical features that have high enough probability ratios and large enough support. We propose a histogram-based approach that initiates a value interval by a specified grid and iteratively expands the interval to its neighbour grids when certain criteria are met.

This process begins with a binning step that divides the value range of a feature into a number of grids n_g . We offer a few options for the binning strategy in our implementation, including “uniform”, “kmeans”, and “quantile”. The “uniform” strategy ensures all grids in each feature have identical widths; “kmeans” assigns values in each grid have the same nearest centre of a 1D k-means cluster; “quantile” results in grids with an equal number of points across each feature. We found that the “uniform” and “kmeans” strategies work better than “quantile” in all of our experiments.

Intuitively, we should start with a peak grid that gives the highest ratio \mathbf{r}_{f_i} and expand it when possible. Nonetheless, this might not be able to find the optimal interval if the ratios in its neighbour grids decrease rapidly. An example is demonstrated in Figure 4(b), in which the peak grid in the interval \mathbb{X}_a is higher than the peak grid in the interval \mathbb{X}_b , however, the overall ratio of the interval \mathbb{X}_a is lower than the overall ratio of the interval \mathbb{X}_b . It is also possible that there exist multiple intervals with similar ratios and we can not know which one is better before finishing the search for a whole rule set. Considering such multi-mode scenarios, we search intervals that start with every peak grid and choose candidate

intervals with the top K ratios. We implemented a simple method based on first-order derivatives to find peaks of the ratio histogram, which can be replaced by more advanced methods. We only select peak grids with a ratio larger than 1. Here we choose the same K as in Algorithm 3.

Algorithm 4 GetCandidateRules

Input: X – features of training samples; f – index of the specific feature; Y – indicator of the target region $y \in \mathbb{Y}$, which is a binary vector; \mathcal{X}_{pre} – previous rules; s_{min} – minimum support of a rule set; n_g – number of value grids for numerical features; K – maximum number of candidate rules.

$\mathbf{x}_g^f \leftarrow$ get n_g value grids of f -th feature
 $\mathbf{r}_g \leftarrow$ Calculate probability ratios of each grids (Equation (7)),
 $\mathbf{s}_g \leftarrow$ Calculate supports of each grids,
 $\mathbf{x}_g^f, \mathbf{r}_g, \mathbf{s}_g \leftarrow$ Merge consecutive grids with identical ratios, merge empty grids to its neighbour grid with a higher ratio,
 $\mathbf{g}_p \leftarrow$ Get peak grids with ratio peaks larger than 1 and sort them by their ratios,
 $\mathbb{X}_f, \mathbf{r}_f \leftarrow$ Generate candidate rules for f -th feature by Algorithm 5, starting with every grids in \mathbf{g}_p .
Return: K rules in \mathbb{X}_f with top K ratios in \mathbf{r}_f

After initiating an interval by specifying a peak grid, we then expand it by the following criteria:

- i) when the support of this interval is smaller than the minimum support s_{min} we expand the interval to its neighbour grids if possible;
- ii) when the support of this interval is not smaller than s_{min} , we only expand the interval to a neighbour grid when this neighbour grid has a higher ratio. This will guarantee that an interval with enough support only expands when its ratio gets increased (Proposition 1).

The pseudo-code of this rule generation process for numerical features are described in Algorithms 4 and 5. Figure 4(c) visualises this process with synthetic data in a 2-dimensional feature space.

Additionally, we provide local rule extraction for a given sample (as demonstrated in Table 2), which forces the value interval of a feature to include the feature value of a given sample. If the feature intervals obtained by Algorithms 4 and 5 do not meet this requirement, we apply a local

Algorithm 5 GenFeatureInterval

Input: s_{min} – minimum support of a rule set, g_p – index of a peak grid to initiate an interval; \mathbf{x}_g – value grids of a feature; \mathbf{r}_g – probability ratios of value grids; \mathbf{s}_g – supports of value grids; Y – indicator of the target region $y \in \mathbb{Y}$, which is a binary vector; \mathcal{X}_{pre} – previous rules.

$\mathbb{X}_{f,p}, s, r \leftarrow$ Initialise an interval by the peak grid g_p and its support $\mathbf{s}_g[g_p]$, ratio $\mathbf{r}_g[g_p]$,
while $s < s_{min}$ or $r > 1$ **do**
 if $s < s_{min}$ **then**
 $\mathbb{X}_{f,p}, s, r \leftarrow$ Expand the interval to a neighbour grid that has a larger ratio than the other neighbour grid,
 else if $r > 1$ **then**
 $\mathbb{X}_{f,p}, s, r \leftarrow$ Expand the interval to a neighbour grid that has a higher ratio than the other neighbour grid and also higher than r . If no such grid exists, break.
 end if
 end while
 if $s < s_{min}$ or $r \leq 1$ **then**
 $\mathbb{X}_{f,p} = \emptyset$
 end if
Return: $\mathbb{X}_{f,p}, r, s$

searching process. This can be directly achieved by starting with the grid that includes the given sample. The local rule extraction may not be able to obtain any valid rules (i.e. the ratios of any value intervals are not greater than 1) if the given sample is an outlier of the target region.

Proposition 1. *Given two exclusive intervals of a feature: $\mathbb{X}_a, \mathbb{X}_b$, where $\mathbb{X}_a \cap \mathbb{X}_b = \emptyset$, and their corresponding ratios $\mathbf{r}_a, \mathbf{r}_b$, if $0 \leq \mathbf{r}_a < \mathbf{r}_b$, then the merged interval $\mathbb{X}_m = \mathbb{X}_a \cup \mathbb{X}_b$ has a ratio \mathbf{r}_m that satisfies $\mathbf{r}_a < \mathbf{r}_m < \mathbf{r}_b$.*

Proof. We first rewrite the density ratio as $\mathbf{r}_a = \alpha_a/\beta_a$, $\mathbf{r}_b = \alpha_b/\beta_b$, where α_a, α_b are non-negative integers, β_a, β_b are positive integers. According to Equation (6), then we have $\mathbf{r}_m = (\alpha_a + \alpha_b)/(\beta_a + \beta_b)$. So we can have:

$$\begin{aligned} \mathbf{r}_m - \mathbf{r}_a &= \frac{\alpha_a + \alpha_b}{\beta_a + \beta_b} - \frac{\alpha_a}{\beta_a} \\ &= \frac{\alpha_b - \alpha_a}{\beta_a + \beta_b} \frac{\beta_b}{\beta_a} = \frac{\frac{\alpha_b}{\beta_b} - \frac{\alpha_a}{\beta_a}}{\frac{\beta_a}{\beta_b} + 1} > 0 \end{aligned}$$

Similarly, we can prove $\mathbf{r}_m - \mathbf{r}_b < 0$, which completes the proof. \square

Data availability

The Diabetes prediction dataset is available on: <https://www.kaggle.com/datasets/iammustafatz/diabetes-prediction-dataset>. The sepsis dataset is available on: <https://physionet.org/content/challenge-2019/1.0.0/>. The Tox21 challenge dataset is available on: <https://deepchemdata.s3-us-west-1.amazonaws.com/datasets/tox21.csv.gz>. The MNIST dataset is available on: <http://yann.lecun.com/exdb/mnist/>. The brain tumour MRI dataset is available on: <https://www.kaggle.com/datasets/thomasdubail/brain-tumours-256x256/>.

Code availability

All source code is available on: <https://github.com/tmi-lab/AMORE>. The libraries and their versions and dependencies that are used in the code are also provided as a separate configuration file in JSON/YAML format. The code is available under the CC-BY-4.0 license.

References

- [1] Arrieta, A.B., Díaz-Rodríguez, N., Del Ser, J., Bennetot, A., Tabik, S., Barbado, A., García, S., Gil-López, S., Molina, D., Benjamins, R., *et al.*: Explainable artificial intelligence (XAI): Concepts, taxonomies, opportunities and challenges toward responsible ai. *Information fusion* **58**, 82–115 (2020)
- [2] Hailesilassie, T.: Rule extraction algorithm for deep neural networks: A review. *arXiv preprint arXiv:1610.05267* (2016)
- [3] He, C., Ma, M., Wang, P.: Extract interpretability-accuracy balanced rules from artificial neural networks: A review. *Neurocomputing* **387**, 346–358 (2020)
- [4] Grosan, C., Abraham, A., Grosan, C., Abraham, A.: Rule-based expert systems. *Intelligent systems: A modern approach*, 149–185 (2011)
- [5] Benet, L.Z., Hosey, C.M., Ursu, O., Oprea, T.I.: Bddcs, the rule of 5 and drugability. *Advanced drug delivery reviews* **101**, 89–98 (2016)
- [6] Sutton, R.T., Pincock, D., Baumgart, D.C., Sadowski, D.C., Fedorak, R.N., Kroeker, K.I.: An overview of clinical decision support systems: benefits, risks, and strategies for success. *NPJ digital medicine* **3**(1), 17 (2020)
- [7] Haixiang, G., Yijing, L., Shang, J., Mingyun, G., Yuanyue, H., Bing, G.: Learning from class-imbalanced data: Review of methods and applications. *Expert systems with applications* **73**, 220–239 (2017)
- [8] Mustafa, M.: Diabetes prediction dataset (2023). <https://www.kaggle.com/datasets/iammustafatz/diabetes-prediction-dataset>
- [9] Interpretable Machine Learning, 2nd edn. Lulu.com (2023). <https://christophm.github.io/interpretable-ml-book/>
- [10] Liu, B., Hsu, W., Ma, Y.: Integrating classification and association rule mining. In: *Proceedings of the Fourth International Conference on Knowledge Discovery and Data Mining*, pp. 80–86 (1998)
- [11] Luo, G.: Automatically explaining machine learning prediction results: a demonstration on type 2 diabetes risk prediction. *Health information science and systems* **4**, 1–9 (2016)
- [12] Agrawal, R., Imielinski, T., Swami, A.: Mining association rules between sets of items in large databases. In: *Proceedings of the 1993 ACM SIGMOD International Conference on Management of Data*, pp. 207–216 (1993)
- [13] Agrawal, R., Srikant, R., *et al.*: Fast algorithms for mining association rules. In: *Proc. 20th Int. Conf. Very Large Data Bases, VLDB*, vol. 1215, pp. 487–499 (1994). Santiago, Chile
- [14] Sethi, K.K., Mishra, D.K., Mishra, B.: Kdruleex: A novel approach for enhancing user comprehensibility using rule extraction.

In: 2012 Third International Conference on Intelligent Systems Modelling and Simulation, pp. 55–60 (2012). IEEE

[15] Wang, F., Rudin, C.: Falling rule lists. In: Artificial Intelligence and Statistics, pp. 1013–1022 (2015). PMLR

[16] Yang, H., Rudin, C., Seltzer, M.: Scalable bayesian rule lists. In: International Conference on Machine Learning, pp. 3921–3930 (2017). PMLR

[17] Wang, T., Rudin, C., Doshi-Velez, F., Liu, Y., Klampfl, E., MacNeille, P.: A bayesian framework for learning rule sets for interpretable classification. *Journal of Machine Learning Research* **18**(70), 1–37 (2017)

[18] C4.5: Programs for Machine Learning. Elsevier (2014)

[19] De'ath, G., Fabricius, K.E.: Classification and regression trees: a powerful yet simple technique for ecological data analysis. *Ecology* **81**(11), 3178–3192 (2000)

[20] Sato, M., Tsukimoto, H.: Rule extraction from neural networks via decision tree induction. In: IJCNN'01. International Joint Conference on Neural Networks. Proceedings (Cat. No. 01CH37222), vol. 3, pp. 1870–1875 (2001). IEEE

[21] Wu, M., Parbhoo, S., Hughes, M., Kindle, R., Celi, L., Zazzi, M., Roth, V., Doshi-Velez, F.: Regional tree regularization for interpretability in deep neural networks. In: Proceedings of the AAAI Conference on Artificial Intelligence, vol. 34, pp. 6413–6421 (2020)

[22] Frosst, N., Hinton, G.: Distilling a neural network into a soft decision tree. arXiv preprint arXiv:1711.09784 (2017)

[23] Reyna, M.A., Josef, C., Seyedi, S., Jeter, R., Shashikumar, S.P., Westover, M.B., Sharma, A., Nemat, S., Clifford, G.D.: Early prediction of sepsis from clinical data: the physionet/computing in cardiology challenge 2019. In: 2019 Computing in Cardiology (CinC), p. 1 (2019). IEEE

[24] Kidger, P., Morrill, J., Foster, J., Lyons, T.: Neural controlled differential equations for irregular time series. *Advances in Neural Information Processing Systems* **33**, 6696–6707 (2020)

[25] Wu, Z., Ramsundar, B., Feinberg, E.N., Gomes, J., Geniesse, C., Pappu, A.S., Leswing, K., Pande, V.: Moleculenet: a benchmark for molecular machine learning. *Chemical Science* **9**(2), 513–530 (2018)

[26] LeCun, Y., Cortes, C., Burges, C.: Mnist handwritten digit database. ATT Labs [Online]. Available: <http://yann.lecun.com/exdb/mnist> **2** (2010)

[27] Chitnis, S., Hosseini, R., Xie, P.: Brain tumor classification based on neural architecture search. *Scientific reports* **12**(1), 19206 (2022)

[28] Tan, M., Le, Q.: Efficientnet: Rethinking model scaling for convolutional neural networks. In: International Conference on Machine Learning, pp. 6105–6114 (2019). PMLR

[29] Russakovsky, O., Deng, J., Su, H., Krause, J., Satheesh, S., Ma, S., Huang, Z., Karpathy, A., Khosla, A., Bernstein, M., Berg, A.C., Fei-Fei, L.: ImageNet Large Scale Visual Recognition Challenge. *International Journal of Computer Vision (IJCV)* **115**(3), 211–252 (2015) <https://doi.org/10.1007/s11263-015-0816-y>

[30] Kola, I., Landis, J.: Can the pharmaceutical industry reduce attrition rates? *Nature Reviews Drug Discovery* **3**(8), 711–716 (2004)

[31] Veličković, P., Cucurull, G., Casanova, A., Romero, A., Lio, P., Bengio, Y.: Graph attention networks. arXiv preprint arXiv:1710.10903 (2017)

[32] RDKit Contributors: RDKit: Open-source cheminformatics. <https://www.rdkit.org> (2023)

[33] Sundararajan, M., Taly, A., Yan, Q.: Axiomatic attribution for deep networks. In:

International Conference on Machine Learning, pp. 3319–3328 (2017). PMLR

- [34] Lundberg, S.M., Lee, S.-I.: A unified approach to interpreting model predictions. Advances in neural information processing systems **30** (2017)
- [35] Ribeiro, M.T., Singh, S., Guestrin, C.: "why should i trust you?" explaining the predictions of any classifier. In: Proceedings of the 22nd ACM SIGKDD International Conference on Knowledge Discovery and Data Mining, pp. 1135–1144 (2016)
- [36] Crabbé, J., Qian, Z., Imrie, F., Schaar, M.: Explaining latent representations with a corpus of examples. Advances in Neural Information Processing Systems **34**, 12154–12166 (2021)
- [37] Han, J., Pei, J., Yin, Y.: Mining frequent patterns without candidate generation. ACM sigmod record **29**(2), 1–12 (2000)

Competing interests

The authors declare no competing interests.

Acknowledgements

This study is funded by the UKRI Engineering and Physical Sciences Research Council (EPSRC) PROTECT Project (grant number: EP/W031892/1), and the UK Dementia Research Institute (UKDRI) Care Research and Technology Centre funded by the Medical Research Council (MRC), Alzheimer’s Research UK, Alzheimer’s Society (grant number: UKDRI-7002). Infrastructure support for this research was provided by the NIHR Imperial Biomedical Research Centre (BRC) and the UKRI Medical Research Council (MRC). The funders were not involved in the study design, data collection, data analysis or writing the manuscript.

Author contributions

Y.C. and P.B. conceptualised the study. Y.C. developed the method and drafted the manuscript. T.C. conducted molecular toxicity experiments and contributed to the writing. A.C. assisted with visualisation and open-sourcing the code. N.F. contributed to the writing. All authors reviewed the manuscript.

